Received: 16 September 2019 | Accepted: 14 March 2020

DOI: 10.1002/jmv.25769

RESEARCH ARTICLE

JOURNAL OF MEDICAL VIROLOGY WILEY

Development of hepatic pathology in GBV-B-infected red-bellied tamarins (*Saguinus labiatus*)

Jessica M. Dale[1] | Simon P. Hood[1] | Ori Bowen[1] | Helen Bright[2] | Keith L. Cutler[1] | Neil Berry[1] | Neil Almond[1] | Robert Goldin[3] | Peter Karayiannis[4] | Nicola J. Rose[1]

[1]Division of Virology, National Institute for Biological Standards and Control, Medicine and Healthcare products Regulatory Agency, Blanche Lane, South Mimms, Potters Bar, Hertfordshire, UK

[2]Internal Medicine Research Unit, Pfizer Research and Development, Sandwich, Kent, UK

[3]Department of Cellular Pathology, Imperial College London, St. Mary's Campus, Norfolk Place, London, UK

[4]Department of Medicine, Imperial College London, St. Mary's Campus, Norfolk Place, London, UK

Correspondence
Nicola J. Rose, Division of Virology, National Institute for Biological Standards and Control, Medicine and Healthcare products Regulatory Agency, Blanche Lane, South Mimms, Potters Bar, Hertfordshire EN6 3QG, UK.
Email: nicola.rose@nibsc.org

Present address
Jessica M. Dale, Nottingham Trent University, Clifton, Nottingham, NG11 8NS, UK.

Simon P. Hood, Clinical and Experimental Pharmacology Group, CRUK Manchester Institute, University of Manchester, Manchester, SK10 4TG, UK.

Helen Bright, MedImmune UK Ltd, Renaissance Way, Speke Boulevard, Speke, Liverpool, Merseyside, L24 9JW, UK.

Peter Karayiannis, St George's, University of London Medical Program at the University of Nicosia, 93, Agiou Nikolaou Street, Engomi, PO Box 24005, Nicosia2408, Cyprus.

Funding information
UK Medical Research Council, Grant/Award Number: G0900861; EU FP7, Grant/Award Number: EUPRIM-Net II

Abstract

GB virus B (GBV-B) is a new world monkey-associated flavivirus used to model acute hepatitis C virus (HCV) infection. Critical for evaluation of antiviral or vaccine approaches is an understanding of the effect of HCV on the liver at different stages of infection. In the absence of longitudinal human tissue samples at defined time points, we have characterized changes in tamarins. As early as 2 weeks post-infection histological changes were noticeable, and these were established in all animals by 6 weeks. Despite high levels of liver-associated viral RNA, there was reversal of hepatic damage on clearance of peripheral virus though fibrosis was demonstrated in four tamarins. Notably, viral RNA burden in the liver dropped to near undetectable or background levels in all animals which underwent a second viral challenge, highlighting the efficacy of the immune response in removing foci of replication in the liver. These data add to the knowledge of GBV-B infection in New World primates which can offer attractive systems for the testing of prophylactic and therapeutic treatments and the evaluation of their utility in preventing or reversing liver pathology.

KEYWORDS
animal models of infection, hepatitis virus, local infection, replication, spread

1 | INTRODUCTION

Infection with hepatitis C virus (HCV) remains a worldwide public health issue. While there have been recent advances in novel direct-acting antivirals (DAA), the availability and accessibility of these globally is not certain. The long-term effects such as viral resistance and side-effects are not yet established. Further, a crucial target population—those unaware of their infection status—is not easily defined. Thus, the need remains to implement an effective prophylactic vaccine in a cost-effective manner. While 75% to 85% of infected individuals develop chronic infection, for reasons that are not clear, 15%-25% of HCV-infected individuals appear able to clear their

peripheral viremia. If the mode of control in acute infection was fully understood, then it would provide a guide for the rational design of effective vaccine and treatment strategies. Such a description would need to include liver pathology as well as events detectable in the peripheral blood.

The clinical study of acute HCV is difficult, not only from the challenges of acquiring appropriate information about the liver in a noninvasive manner, but also identifying individuals with inapparent infections in the absence of compromising concomitant infections or lifestyles. Model systems of HCV infection are also imperfect, whether it be in chimpanzees or humanized mice. As a result, we and others have explored surrogate models.

GB virus B (GBV-B) is a flavivirus phylogenetically and functionally closely related to HCV and known to infect New World primates.[1] The authors noted that infection of owl monkeys (family *Aotidae*) resulted in lower peak viral titers and lower incidence of viral hepatitis than seen in tamarins (family *Callitrichidae*). Experimental infection with GBV-B results in high viremia, typically followed by a viral clearance from the periphery within 18 weeks of infection (reviewed in Reference 2); rechallenge following clearance is typically readily controlled.[3] The potential utility of a New World primate *Hepacivirus* model in the investigation of liver-associated pathology concomitant with peripheral viremia is highly important. In characterizing early liver pathology, the effect of candidate immunotherapies may then be evaluated not only against the control of circulating viral RNA but also the prevention or reversal of virus-associated damage to the liver.[4]

Few studies on the histology and immunopathology of GBV-B have been reported but these include both marmosets and tamarins. Hepatitis in the marmoset was characterized at 4 weeks post-infection by a large number of infiltrating $CD3^+$ cells within portal tracts and hepatic parenchyma and $CD20^+$ cells in the portal tracts, though there was an absence of $CD4^+$ cells.[5] We and others have shown that in both the tamarin and marmoset models, $CD8^+$ T cells have been shown to produce interferon-γ (IFN-γ) in response to peptide stimulation with nonstructural proteins.[6,7] A number of immunohistochemical and histopathological studies have been reported for the marmoset,[5,6,8,9] but fewer for tamarins.[10-12] Martin and colleagues noted a single tamarin at 107 weeks post-infection (wpi) with lymphocyte infiltrate within expanded portal tracts, filtering into the parenchyma, confirmed that tamarins are capable of developing ongoing hepatitis.[11] To date, complications that are associated with HCV infection such as fibrosis have only been reported in marmosets challenged with either GBV-B alone[8,9,13] or chimeric GBV-B/HCV in the presence or absence of an immunosuppressant, FK506.[14,15] Knowledge of the comparative pathology between tamarin and marmoset as a result of Hepacivirus infection would highlight advantages in the use of either species.

We have expanded on previous reports in which pathology at defined time points has been assessed. Here, we have characterized the progression of GBV-B-associated liver pathology by immunohistochemistry in 18 red-bellied (white-lipped; *Saguinus labiatus*) tamarins to provide the first longitudinal study of pathology development. In the early stages of infection, tissue morphology was broadly unchanged but there was an advanced degree of immune infiltrate in the liver. A range of liver dysmorphia and immune infiltrate was seen in animals convalescent from primary infection. In the ten animals subjected to a secondary exposure to GBV-B, liver immunopathology on termination was advanced in those animals receiving a higher dose of virus. Importantly, we report for the first time that, akin to the genus *Callithrix* (Atlantic marmosets), acutely-infected red-bellied tamarins (*Saguinus labiatus*; genus *Saguinus mystax*) are capable of developing fibrosis following GBV-B infection which mimics disease progression often associated with chronic HCV infection. Thus the GBV-B/tamarin model remains a valid model to support research into hepacivirus infection[2] and further offers an opportunity to study virus-induced liver pathology, including fibrosis development. We have demonstrated that it could be utilized to evaluate the ability of novel prophylactic and therapeutic treatments to prevent or reverse viremia and liver damage. Such information could inform the clinical application of these treatments in humans with HCV infection.

2 | MATERIALS AND METHODS

2.1 | Animals and biological samples

Purpose-bred, weaned (and less than 24 months of age), red-bellied tamarins (*Saguinus labiatus*) were housed, and all animal procedures were performed in strict accordance with UK Home Office guidelines, under a licence granted to the host establishment by the Secretary of State for the Home Office which approved the work described. Tamarins were group-housed in same-sex groups for the duration of the study, with daily feeding and access to water ad libitum. Of the 18 tamarins, 10 were male and 8 were female. Animals were weighed weekly: pre-study weights of males ranged from 541 to 770 g (mean, 682 g; median 669 g); pre-study weights for females ranged from 441 to 837 g (mean, 678 g; median, 684 g). The availability of tamarins precluded age, sex, and weight matching but this was not central to the study outcome. Regular modifications to the housing area and environmental enrichment were made by husbandry staff. The environmental temperature was appropriate for tamarins and rooms were subject to a 12-hour day/night cycle of lighting. Animals were acclimatized to their environment and deemed to be healthy by the named veterinary surgeon before inclusion in the study.

All animals were inoculated with a stock of GBV-B-infected serum derived from the original ATCC inoculum after serial passage through two red-bellied tamarins. All surgical procedures were performed under anesthesia with recovery. Animals were bled through the femoral vein and serum separated. Where required a liver section (wedge biopsy) (approximately 5 mm^3) was removed at a single time point during infection by surgical laparotomy with recovery, and further samples were available at termination. Liver sections were fixed in 10% formalin and embedded in paraffin wax using a Leica ASP100 automated processor. Sections (4 μm) of each tissue were cut and mounted onto glass slides. Before any treatment, all slides

were deparaffinated using xylene (Fisher Scientific UK Ltd, Leicestershire, UK) and rehydrated using an ethanol series.

Groups of tamarins were treated thus: Group A: six tamarins (S2, S3, T20, V6 [male] and T18, V2 [female]) were infected with 1×10^7 genome equivalents (ge) GBV-B. A liver section was taken at 2 wpi, with recovery. Following a period of undetectable peripheral viremia, the tamarins underwent challenge with homologous virus; 1×10^7 ge GBV-B. Group B: four tamarins (W1, W2, W4, W11; all female) were infected with 1×10^7 ge GBV-B and terminated 6 wpi. Group C: four tamarins (V7, V8, W3, W5; all male) were infected with 1×10^7 ge GBV-B and terminated approximately 26 wpi when peripheral viremia had been undetectable for a minimum of 2 weeks. Group D: four tamarins (T10, V1 [female] and T21, V3 [male]) were infected with 1×10^5 ge GBV-B. A liver section was taken at 2 wpi, with recovery. Following a period of undetectable peripheral viremia, the tamarins underwent a challenge with the homologous virus, 1×10^5 ge GBV-B. Group E: Tissues from four tamarins (F21, G13, M7, P6) not infected with GBV-B (naïve) were available for this study from an archive of such materials, thus reducing the need for additional animals for the study.

Infection profiles for Groups B and C tamarins have been reported previously.[7] Virus inoculum for all animals was identical.

2.2 | Viral load quantification

Viral RNA was isolated from serum using the QIAamp viral RNA extraction kit (Qiagen) according to the manufacturer's instructions. Quantification of the GBV-B genome was performed by real-time PCR using a method adapted from Beames et al.[16] GBV-B Core sequences were quantified in duplicate using the RNA Ultrasense One-step qRT-PCR system on a MX3000P system (Stratagene). Primers 558F (5′-AAC GAG CAA AGC GCA AAG TC-3′) and 626R (5′-CAT CAT GGA TAC CAG CAA TTT TGT-3′) were used at a concentration of 400 and 900 nM, respectively. A dual-labelled probe (5′ FAM-AGC GCG ATG CTC GGC CTC GTA AT-BHQ1 3′) was used at a concentration of 200 nM. Reverse transcription consisted of a single incubation at 50°C for 15 minutes followed by 40 cycles of DNA amplification comprising 95°C at 1 minute, 62°C at 30 seconds and 72°C at 30 seconds. Standards used to determine genome equivalents were derived from synthetic GBV-B Core RNA in vitro transcribed from a plasmid using the MEGAscript SP6 Kit (Ambion). The limit of quantification of the assay was 10^2 ge/mL.

Liver tissue taken from animals at termination was available for the quantification of GBV-B vRNA. Total RNA was extracted from a 0.5 cm^3 frozen section of liver in 1 mL RLT buffer (Qiagen RNeasy Mini Kit; Qiagen, UK). The tissue samples were placed into Precellys 24 homogenization tubes (Peqlab, UK), and homogenization was performed using a Precellys 24 cell lysis and tissue homogenizer (Bertin Technologies, France). A program of 2×20 seconds at 3000 *g* was used. RNA was purified from the homogenate using the RNeasy Mini Kit (Qiagen) following the manufacturer's instructions. RNA was quantified and the concentration adjusted to 0.2 μg/μL. vRNA was quantified as described for serum vRNA levels and titers expressed per 400 ng total RNA (equating to approximately 10 000-15 000 cells). The limit of quantification was 7.6×10^2 copies/400 ng total RNA.

2.3 | Quantification of serum liver enzymes

Alanine aminotransferase (ALT) is the primary biomarker of liver injury, however in studies of human liver damage glutamate dehydrogenase (GLDH) correlated highly with ALT across a range of disease permutations. GLDH is also a more liver-specific biomarker and thus a more clinically informative indicator of liver disease.[17] To indirectly assess liver damage, serum levels of ALT and GLDH were measured using a Kodak Ektachem automated analyzer (Kodak Ltd UK Suppliers, Orthochemical Diagnostics, Amersham, UK). Pre-infection samples were also assessed for each animal.

2.4 | Assessment of tissue morphology

To assess general morphology, sections were incubated in Harris' hematoxylin (Thermo Fisher Scientific, UK) for 15 minutes, followed by 1% acid alcohol (1% HCl in 70% IMS) for 40 seconds and counterstained with eosin (Thermo Fisher Scientific) for 10 minutes. Excess stain was removed using distilled H_2O. Sections were air-dried and mounted under a coverslip using Locktite superglue. To assess the extent of collagen deposition in tissue, indicative of fibrotic tissue, sections were taken into 0.1% fast green for 10 seconds, washed in distilled H_2O and incubated in 0.1% sirius red for 15 minutes before being dried at 60°C for 15 minutes and mounted using DPX mountant (all Sigma-Aldrich, UK). All data were referenced to sections from GBV-B-naïve tamarins unless stated otherwise.

2.5 | Detection of cellular proteins by immunohistochemistry

Immunohistochemistry (IHC) was performed using a Leica Bond Max processor following the manufacturer's instructions (Leica, UK). Tissue sections were treated with monoclonal or polyclonal antibodies against a range of host proteins using either the "IHC Protocol F-10" or the "ABC 2 Intense R" program. The antibodies were evaluated against tissues from naïve and infected tamarins. Various antibodies, including anti-human clones, demonstrated cross-reactivity with tamarin tissue, and were selected for use. Polyclonal Rabbit CD3 anti-human (A0452; Dako), monoclonal mouse CD4 (Clone 4B12; Vector, UK) and monoclonal mouse CD8 (Clone UCH-T4; Santa Cruz) were used to detect broadly reactive T cells. Monoclonal mouse CD20cy anti-human (Clone L26, M0755; Dako) and monoclonal mouse CD68 anti-human (Clone KP1, M0814; Dako) were used to identify B cells and macrophages, respectively. Polyclonal goat CXCL10 (IP-10; Clone C-19; Santa Cruz) was used as an indirect marker for IFN-γ release. Ki-67 (Clone K2, PA0230; Leica, UK) and monoclonal mouse anti HLA DP, DQ, DR antigen (Clone CR3/43, M0775; Dako) were used to detect cell proliferation and the presence of

MHC Class II as an indirect marker for CD4 responses and B cell regulation, respectively. Secondary antibodies included a universal antibody and an anti-goat antibody (both Leica). All data were referenced to sections from GBV-B-naïve tamarins unless stated otherwise. A lack of cross-reactive antibodies against known tamarin CD markers restricts characterization of the hepatic infiltrate in tamarins and marmosets to the identification of certain T cells and B cells. Data are presented in the results figures with reference to a representative tissue section.

2.6 | Analysis of tissue staining

Following staining each tissue section was visualized using a Nikon Eclipse E400 microscope set to 10 to ×20 magnification using the Metaview software (Meta Imaging software, MDS Analytical Technologies, UK). A scoring index for the breadth of staining present (percentage of stained cells) and intensity of the staining was used, as previously described.[18] The scoring system to determine the extent of fibrosis was the modified histological activity index (HAI[19]).

3 | RESULTS

3.1 | Serum viral load and liver enzymes

All inoculated animals became infected (Figure 1A-D). Data previously reported for animals in Groups B and C[7] are included to facilitate comparison. While most of the animal had viremia profiles that were consistent with published reports, tamarin V1 had viral loads that fluctuated from undetectable to a maximum of approximately 10^7 ge/mL, and tamarin T10 maintained a detectable viral load for nearly 40 weeks. Following challenge with 10^5 ge GBV-B virus was undetectable in the blood of T10 and this animal was terminated 3 wpc as a result of a non-experiment-related injury. Weights fluctuated throughout the study, and transient weight loss was recorded in 12 animals either after first or second challenge. However, there was no overt association of weight gain/loss dynamics and viral burden or hepatic pathology.

Raised serum liver enzyme levels (Figure 1A-D) in animals T20 and V6 (Group A) were not apparent in primary infection but were observed on secondary exposure to virus. In all other Group A and C animals, a rise in ALT and GLDH levels was coincident with the point at which peripheral viremia started to decline. No overt link between levels of enzymes and overall pathology was noted.

3.2 | Liver-associated viral RNA loads

Levels of intracellular vRNA were assessed in all animals at termination (Figure 2). Detectable viral loads were dramatically lower in animals which had cleared their challenge virus. Low levels of virus only, were detectable in just six of the ten tamarins across Groups A and D irrespective of original inoculum dose. vRNA was not detected in naïve tamarins (Group E).

3.3 | Liver immunopathology throughout primary infection, clearance, and rechallenge

Liver pathology for Groups B and C animals has been reported[7]: here detailed analysis facilitates comparison with animals from the other groups (Table 1). Representative images are shown to illustrate the immunostaining patterns (Figure 3). The intensity and breadth of staining is documented in Figure S1.

3.4 | Liver immunopathology associated with GBV-B infection at 2 wpi

Of the animals which received the higher dose inoculum (Group A), immune infiltrate identified by hematoxylin and eosin (H&E) staining was observed in S2 and T18 and to a lesser extent in V6. The remaining Group A animals and Group D animals had minimal morphological changes (data not shown). Lymphocyte infiltration and cell proliferation was observed (Figure 3), as evidenced by slightly elevated levels of CD3, CD4, CD20, and Ki-67 stained cells in three of the six Group A animals (S2, T18 and V6; and V2 for Ki-67 only) and one Group D tamarin (V3). A marginal increase in CD68-stained cell levels was detected in the parenchyma of all animals and the portal tracts of S3 (Group A) and V3 (Group D). Levels of other markers were broadly comparable to those in the naïve animals.

3.5 | Development of liver immunopathology at 6 wpi

Liver sections from three Group B tamarins (W1, W2, and W11) showed only slight lymphocyte infiltration of the portal tracts. Tamarin W4 displayed hepatocyte swelling and lymphocyte infiltration from the portal tracts into the parenchyma (data not shown). By IHC a distinct increase in lymphocyte infiltration (CD3, CD4, and CD20 cells) was observed above that at the 2 wpi time point in both the portal tracts and parenchyma of all animals. The increased level of cell proliferation, as evidenced by Ki-67 staining in all animals, was comparable to that seen in 5 of 10 animals at 2 wpi. Periportal detection of CD8-stained cells and increased cytoplasmic staining for IP-10 in the parenchyma was noted in all animals compared to those studied at 2 wpi. In contrast, staining levels for CD68 cells were unchanged and only a marginal increase in MHCII cells was observed. Images from W4 are shown as representative (Figure 3).

3.6 | Liver immunopathology following acute primary infection

Varying degrees of morphological changes to the liver were observed by H&E staining in the four tamarins terminated at 26 wpi. The greatest morphological changes were noted in W5 (viremia detected to 22 wpi): hepatocyte ballooning, leukocyte infiltrate in the portal

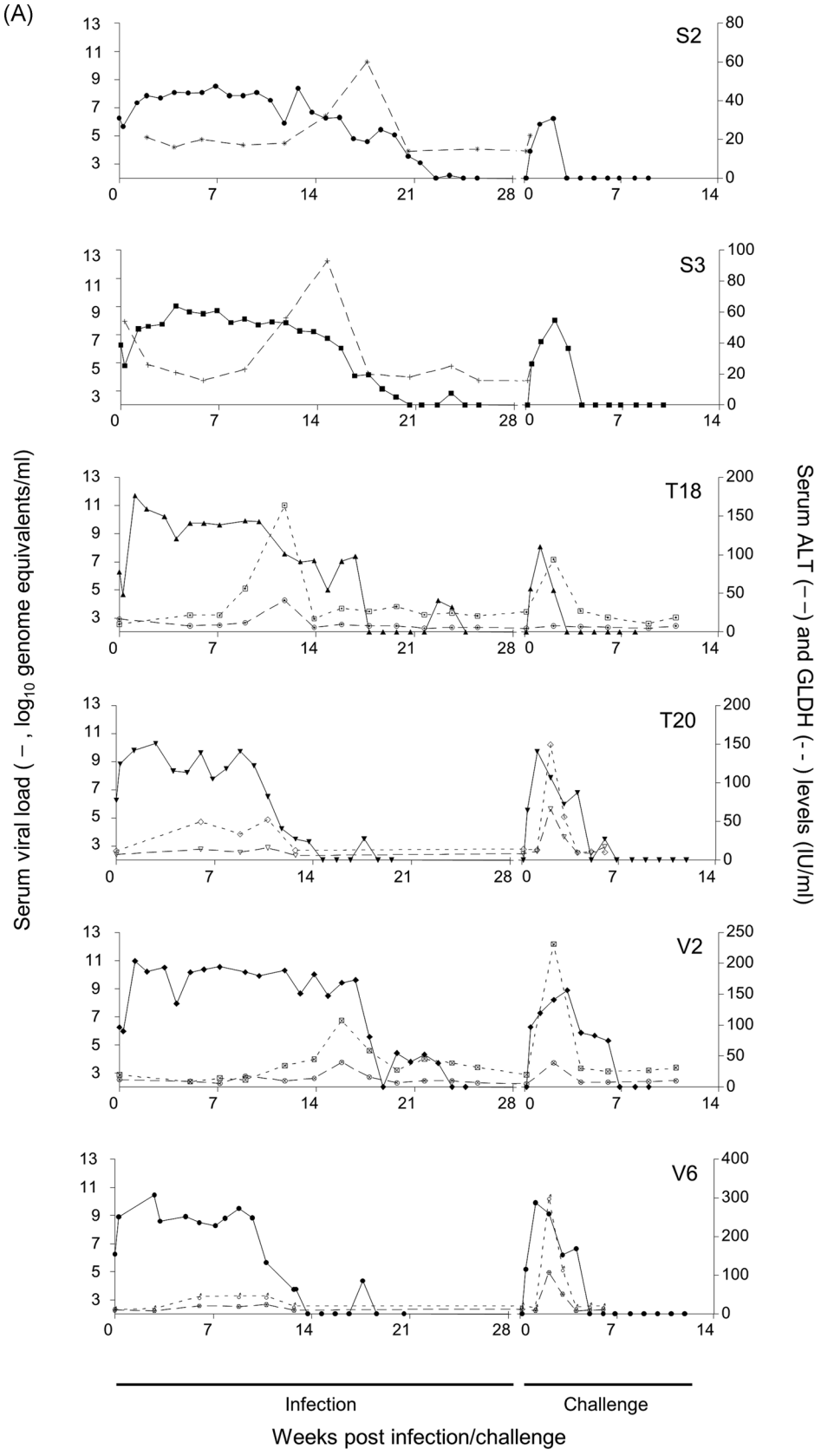

FIGURE 1 Infection profiles for all tamarins during primary infection and challenge. Serum viral loads in $\log_{10}$ genome equivalents per mL (solid line), serum Alanine aminotransferase (ALT) (dotted line), and serum glutamate dehydrogenase (GLDH) (dashed line), both in International Units, are shown for Group A (A), Group B (B), Group C (C), and Group D (D) tamarins

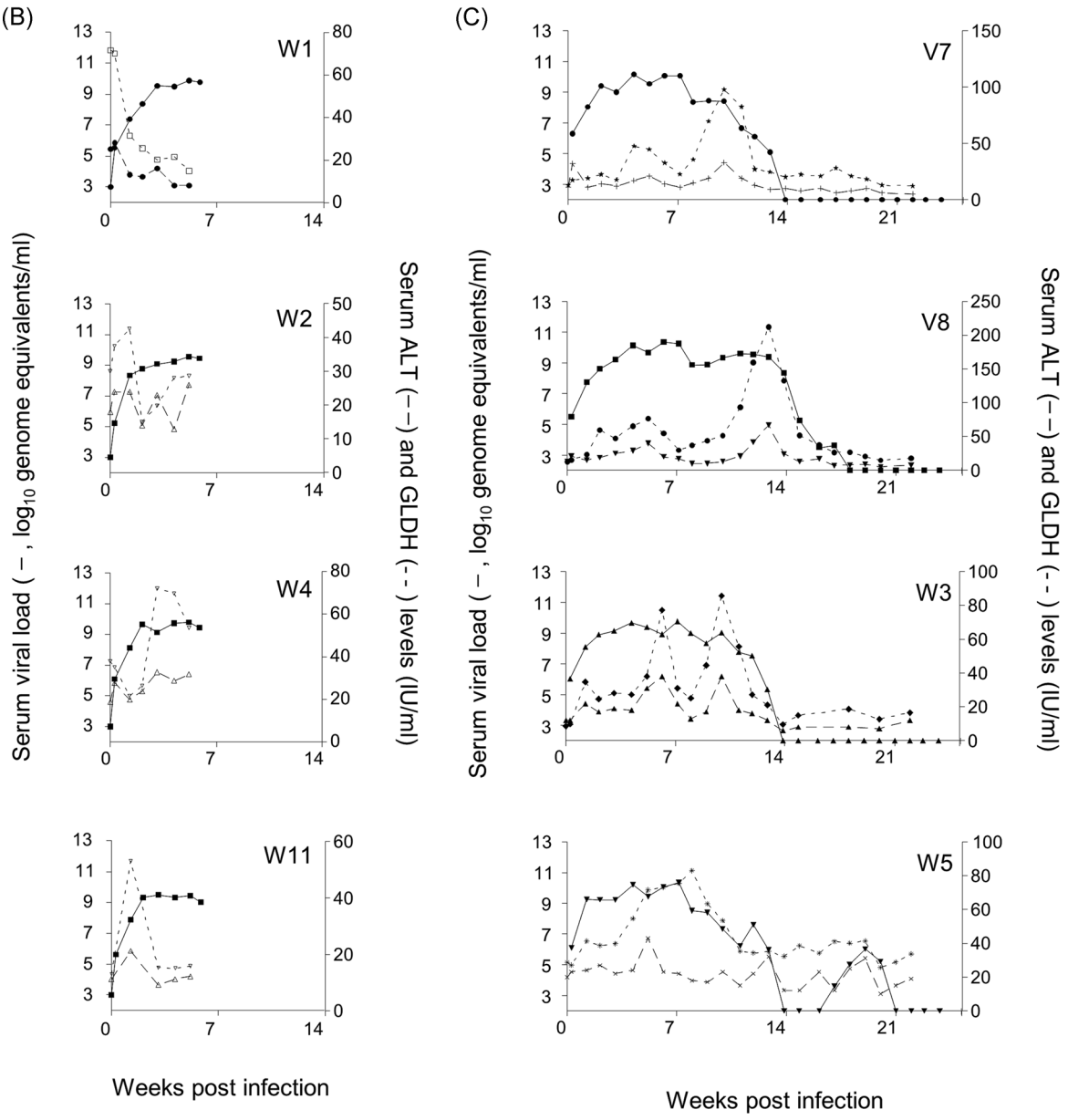

FIGURE 1 (Continued)

tracts and a degree of erythrocyte aggregation in sinusoids. Extensive immune infiltrates of portal tracts and aggregates within swollen sinusoids were shown in the liver of V7 liver (viremia detected to 14 wpi). In contrast, tamarins W3 and V8 (viremia detected to 14 and 19 wpi, respectively) displayed levels of immune infiltrates comparable to naïve tissue (data not shown). Notably, there was an absence of CD3 staining and minimal accumulation of CD4 and CD8-stained cells.

By IHC the greater degree of immune infiltrate staining was seen in W5 and V7 but levels of CD3, CD4, CD68 and IP-10 stained cells in the liver were not greatly above those seen in the naïve tamarins, with some foci of CD4 staining in the portal tracts (Figure 3). CD8, CD68, and CD20 staining levels were comparable to those observed at 6 wpi. V8 and W3 had similar low levels of immunostaining not greatly different from earlier time points (Figure 3; Table 1).

3.7 | Liver immunopathology following clearance of rechallenge virus

At this time point the altered location of stained cells was more apparent when compared with earlier time points. When liver morphology (expansion of the portal tracts and expanded sinusoids containing infiltrating leukocytes in the liver and hepatocyte ballooning) was considered by H&E staining on termination, of the six Group A tamarins infected and challenged with 10^7 ge GBV-B, three (S3, T20, V2) exhibited moderate immunopathological changes and

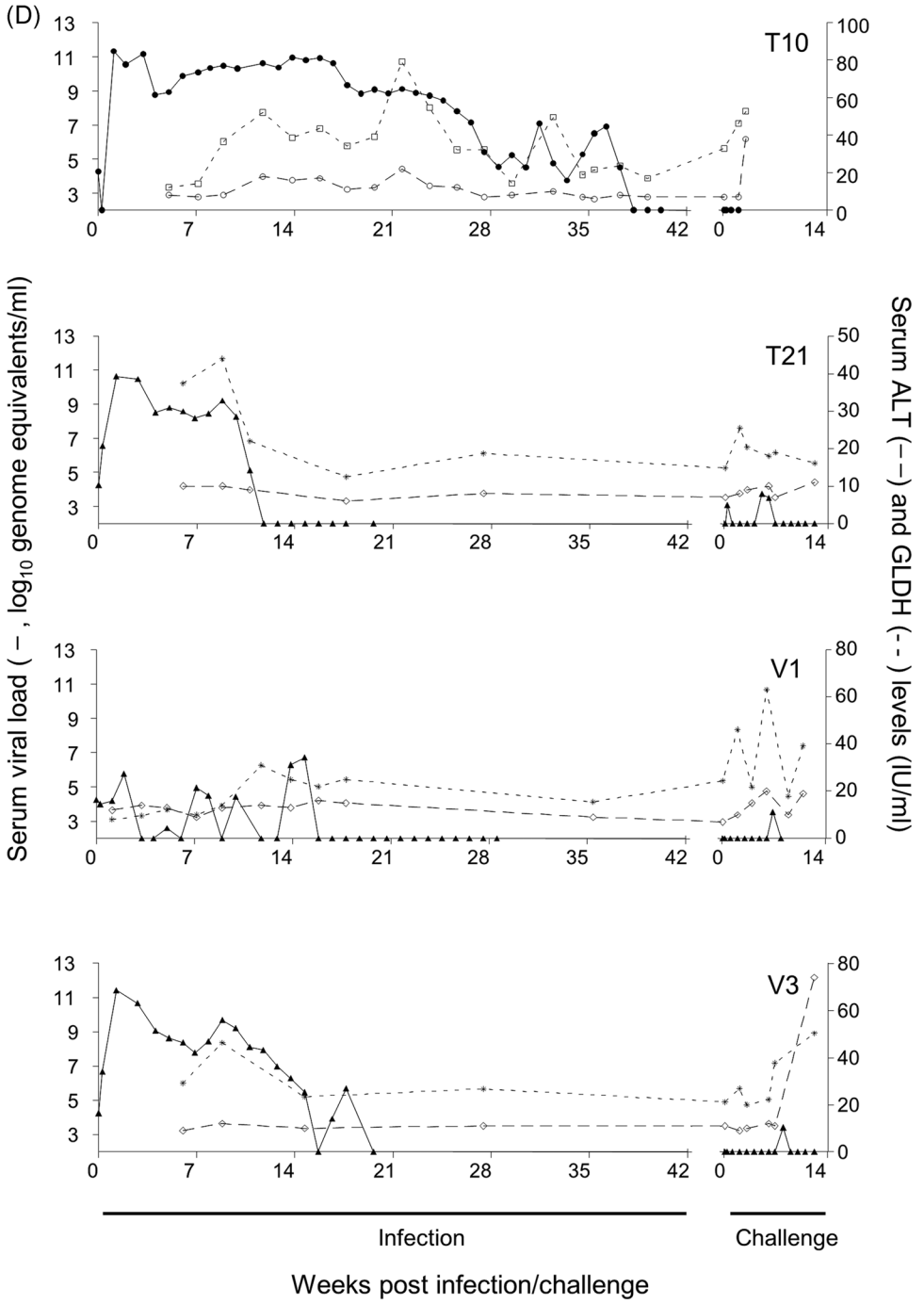

FIGURE 1 (Continued)

three (S2, T18, V6) exhibited extensive liver damage. There were two males and 1 female in each of these categories.

The extensive liver damage in S2, T18, and V6 included hepatocyte ballooning, extended portal tracts and the presence of fat vacuoles. A high degree of extramedullary erythropoiesis (EME) infiltration of the portal tracts, which expanded into the parenchyma and immediate sinusoids was observed (data not shown). These changes did not correlate with cell proliferation levels as evidenced by Ki-67 staining levels which were still high in the portal tracts and parenchyma of 5/6 Group A animals (not V2). Overall, more intense IHC staining levels were observed in these animals (Figure S1). CD3, CD4, and CD20 staining was observed in the portal tracts and parenchyma of all three animals, with the fewest CD4 cells observed in S2 and V6. The CD4 staining pattern was punctate. CD8-stained cells were detected in both the portal tracts and parenchyma of V6, and only in the parenchyma of S2. CD68-stained cells were numerous in the parenchyma of S2 and V6 but fewer were found in the portal tracts. IP-10 cytoplasmic staining was equivalent to that from the

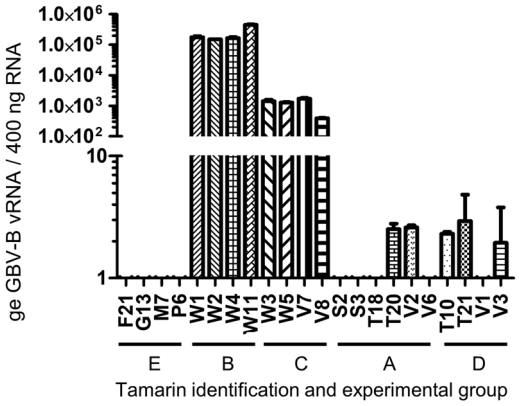

FIGURE 2 Viral load in the liver presented as genome equivalents (ge) of GB virus B (GBV-B) per 400 ng total RNA (approximately 10 000-15 000 cells) for each animal. The limit of quantification was 7.6×10^2 ge/400 ng total RNA. Tamarin identifications within the experimental groups are shown

early time-points but now observed in the parenchyma and portal tracts (Figure 3, Table 1). Of the remaining three tamarins from Group A, animals S3 and T20 had similar staining patterns to those above but with variations on staining intensity and location (Table 1). Animal V2 had high levels of MHCII staining but all other tissues resembled those from the naïve animal.

Of the four tamarins in Group D only a male, T21, demonstrated liver damage (comparable to that in S2 and V6; Group A, males), with portal tract expansion and EME infiltration expanding into the parenchyma. In animal T21, CD3, CD20, and IP-10, positive staining was generally observed in the portal tracts and parenchyma. Cell proliferation (Ki-67 staining) was particularly evident in the portal tracts. There was an absence of CD8 staining, CD4 positive cells were only detected in the portal tracts and CD68 cells were only identified in the parenchyma. T10 (Group D; female) displayed no notable immunopathology. Images from V3 are shown as illustrative of the pathologies post-challenge for the remaining Group B tamarins (Figure 3, Table 1).

3.8 | Development of fibrosis

Evidence of fibrosis was observed in the liver sections from one tamarin terminated at 26 wpi and three which were terminated post-challenge (Figure 4). W5 (Group C; male), was terminated post-primary infection and displayed mild focal portal expansion, scoring 1 on the HAI scale. Immune infiltration of the portal areas was observed. Of the three animals terminated on clearance of the rechallenge virus, T21 (Group D; male) and V6 (Group A; male) showed signs of focal bridging of the portal tracts, scoring 3 on the HAI scale. S2 (Group A; male) displayed extensive fibrosis evidenced by the formation of fibrotic nodules near the portal tracts, in addition to the focal bridging of the portal tracts, and scored 3+ on the HAI scale. The animals that displayed fibrosis had extensive immune infiltration, whereas T18 (female) had had extensive infiltrate but no evidence of fibrosis. None of the animals in Group B (all females) displayed signs of fibrosis. Fibrotic tissue was not observed in naïve tissue.

4 | DISCUSSION

We describe hepacivirus-associated liver pathology development in a New World primate, *Saguinus labiatus* from early GBV-B infection through to secondary challenge by longitudinal study of three tamarin cohorts. Despite high peripheral viral loads, liver morphological changes and lymphocyte infiltrate were minimal at 2 wpi indicating a delayed or low immune response and that structural damage does not necessarily develop at this early stage of infection. Liver sections from three of the four animals terminated 6 wpi displayed broadly normal morphology, comparable levels of immunostaining for assessed markers and high intracellular levels of viral RNA in the liver. While there was evidence of lymphocytes in the portal tracts of one animal (W4) these data suggest an early window during which viral infection could be treated with minimal lasting morphological effects on the liver.

An increased immune infiltrate appeared in the liver by 6 wpi and persisted to post-challenge. This infiltrate typically comprised equal proportions of T and B cells or a slight bias towards CD4 T cells, in contrast to GBV-B infected marmosets,[5] suggesting the involvement of both T-cell subsets in the tamarin response to GBV-B. Increased IP-10 levels occurred in the parenchyma; this cytokine has been shown to attract CXCR3-expressing CD4 and CD8 TH_1 cells in the liver of acute HCV-infected chimpanzees and in chronically-infected HCV patients.[20,21] The return of IP-10 expression to naïve levels in tamarins that cleared GBV-B infection in the periphery at 26 wpi (W5 and V8) coincided with decreased infiltration of both CD4 and CD8 T cells and likely reflects a decrease in IFN stimulation. The CD4 and CD8-stained cells were detected in the absence of CD3 staining suggesting that cells such as NK, macrophage and dendritic cells may be present. These data support our previous observations for isolated intrahepatic lymphocytes.[7] Complexes of suitable antibodies are required to distinguish these cells and in the current absence of such reagents suitable for IHC, this characterization is outwith the scope of this study, though supported by alternate studies.[8]

In the primary infection there was an absence of CD8 cells 2 wpi, while there is a modest increase was observed at 6 and 26 wpi. These data mirror those from the PMBC and intrahepatic lymphocytes of these tamarins.[7] This may suggest a delayed T-cell response in acute infection while an exhausted population may result in the similar lack of CD8 cell accumulation observed at 2 wpc. Control of GBV-B is associated with increased levels of anti-NS3 antibodies (reviewed in Reference 2). We identified CD20 cells as major contributors to the hepatic infiltrate in the tamarins at 26 wpi and post-challenge, supporting an active antibody component to viral control.

By 26 wpi it was evident that varying degrees of morphological damage could still be detected. Tamarins W5 (representative sample, Figure 3) and V7 had morphological damage and immune infiltration of the portal tracts and parenchyma. Increased CD20 B cells suggest a local humoral response. By contrast the livers of W3 and V8 had no signs of immune infiltrate and were morphologically comparable to

TABLE 1 Summary of morphological and immunostaining data from GBV-B-infected tamarins from Groups A-D

			Morphology		Immunostaining							
Time point	Group	ID	H&E	Sirius red	CD3	CD4	CD8	CD20	CD68	IP10	Ki67	MHCII
2 wpi	A	S2	LI +		++	+++		++	(+) P		+	
		S3							(+) P/PT	(+)		
		T18	LI +		++	+		+	(+) P	(+)	++	
		T20							(+) P			
		V2							(+) P		+	
		V6	LI (+)		++	++		+	(+) P		+	
	D	T10							(+) P			
		T21							(+) P			
		V1							(+) P			
		V3			+	+		+	(+) P/PT	(+)	+	
6 wpi	B	W1	LI (+) PT		+++ P/PT	+++ P/PT	+ PP	+++ P/PT	(+)	+ P	+	(+)
		W2	LI (+) PT		+++ P/PT	+++ P/PT	+ PP	+++ P/PT	(+)	+ P	+	(+)
		W4	Swollen hepatocytes; LI from PT to P		+++ P/PT	+++ P/PT	+ PP	+++ P/PT	(+)	+ P	++	(+)
		W11	LI (+) PT		+++ P/PT	+++ P/PT	+ PP	+++ P/PT	(+)	+ P	+	(+)
Post-primary infection	C	V7	LI ++ PT; aggregates in swollen sinusoids			(+) PT	+ PP	+++ P/PT	(+)	(+) P	++	+++
		V8	LI (+)			(+) PT	+ PP	++ P/PT	(+)	(+) P	(+)	++
		W3	LI (+)			(+) PT	+ PP	++ P/PT	(+)	(+) P	(+)	++
		W5	Hepatocyte ballooning, LI PT, erythrocyte aggregation in S	Mild focal portal expansion; LI of P; HAI 1		(+) PT	+/++ PP	+++ P/PT	(+)	(+) P	++	++
Post-challenge	A	S2	Hepatocyte ballooning; extended PT; fat vacuoles; EME ++ in P, S	Fibrotic nodules at PT; focal bridging of PT; HAI 3+	++	+	+ P only	++	(+)	+	++ P/PT	(+)
		S3	+		+++	++	+	+	(+)	+	++ P/PT	(+)
		T18	As S2			+			+	(+)	+++ P/PT	
		T20	+		+++	+		+++		+	++ P/PT	(+)
		V2	+							+		++
		V6	As S2	Focal bridging of PT; HAI 3	++	+		++	+		+++ P/PT	+
	D	T10										
		T21	Comparable to S2	As V6	++ P, PT	+, PT		+ P, PT		++ P, PT	++, PT	++
		V1								+		
		V3			+	+		++	(+)	++	++	+

Note: (+), +, + +, + + +, minimal, mild, moderate, substantial change (morphology, immunostaining) over naïve tissue. Representative images are presented in Figure 3.

Abbreviations: HAI, histology activity index for assessment of fibrosis; LI, lymphocyte infiltration; P, parenchyma; PP, periportal; PT, portal tract; S, sinusoids.

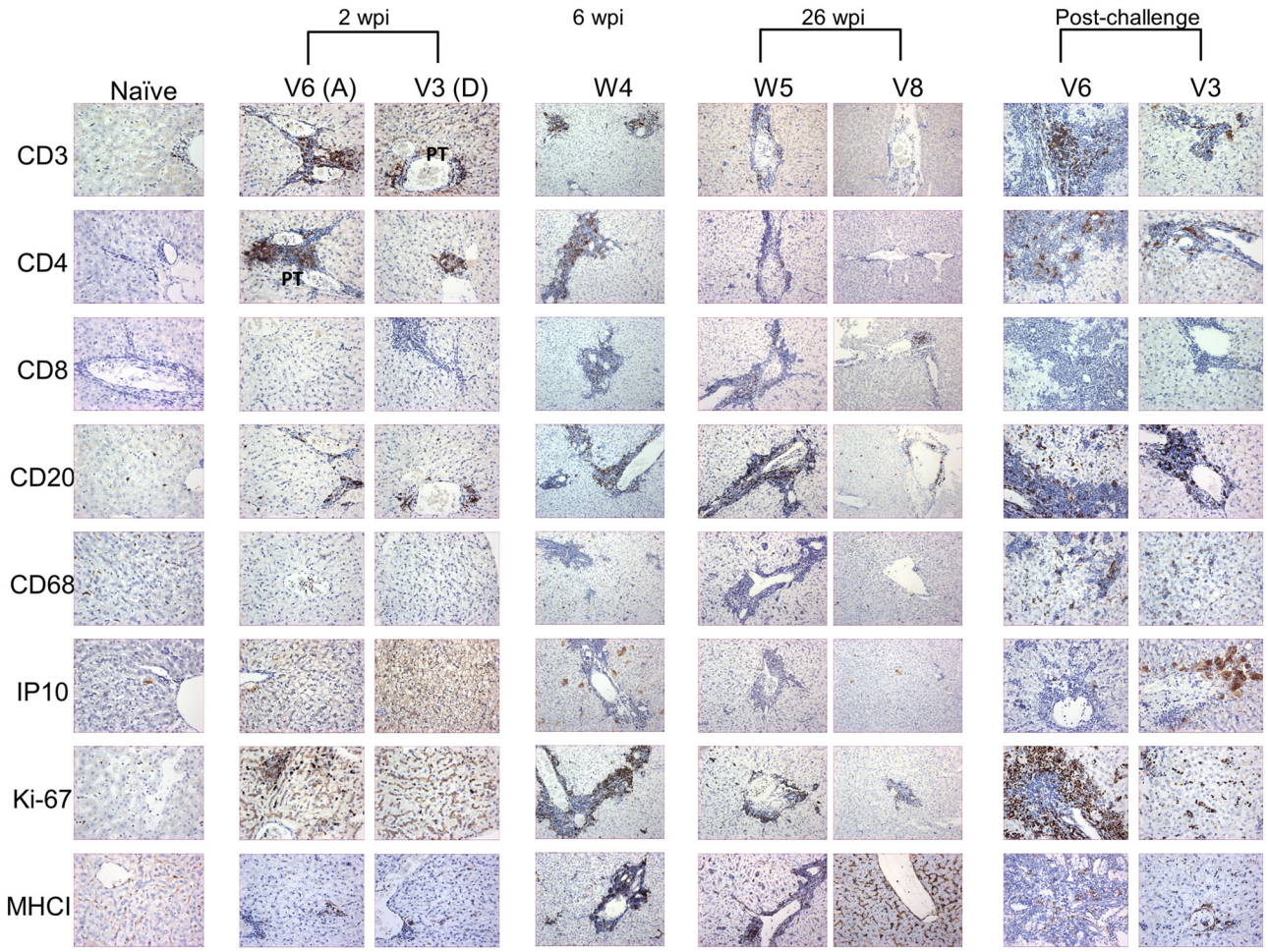

FIGURE 3 Immunohistochemistry staining for eight cell markers is shown for naïve tamarin and for animals representative of different pathologies at 2 wpi (V6, V3; Group indicated), 6 wpi (W4), post-primary infection (W5, V8) and post-challenge (secondary infection; V6, V3). Animals were inoculated with 10^7 ge (V6, W4, W5, V8) or 10^5 ge GBV-B (V3). Positive cells are stained brown. The portal tract (PT) is indicated in two panels for the 2 wpi groups (V6, CD4; V3, CD3). Magnification ×20

the naïve animal suggesting significant reduction of GBV-B in the liver and recovery of normal tissue morphology.

Thus, while it would appear that the livers of some animals may undergo a degree of recovery, the process does not coincide with the absence of peripheral viremia: tamarins V7 and W3 had almost identical peripheral viremia and liver enzyme profiles yet very different liver pathology. With modern DAA treatments this is the benchmark of efficacy, thus recognizing that recovery does not

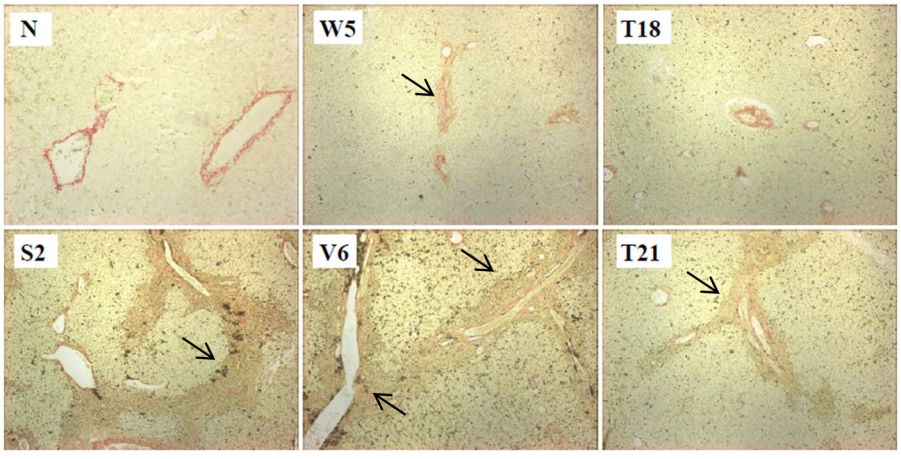

FIGURE 4 Sirius Red staining of collagen is shown for five GB virus B (GBV-B)-infected tamarins and a naïve animal (N). Fibrosis is indicated in the portal tract (arrow) in W5 (post-primary infection; 26 wpi) and in S2, V6 and T21 (post-challenge). Magnification ×10

necessarily coincide with viraemia is of importance. In fact, the presence of considerable levels of intracellular vRNA in the liver suggesting low-level replication of GBV-B, reveals a temporal difference in clearance from the periphery and the liver likely impacting on the recovery of the tissue. Interestingly, even when peripheral virus was undetectable, immune infiltrate and morphological damage were still evident in the liver indicating either a lag between clearance of virus from the liver and tissue repair, or that the virus has yet to be eradicated from the tissue, given that this is the main site of viral replication.

We have previously reported the detection of high levels of vRNA in the liver in the absence of detectable peripheral serum viremia following convalescence from primary viremia.[7] While there have been contrary reports for the occurrence of occult infection in marmosets[6,9]; our observations are consistent with the idea of occult HCV infection in humans (reviewed in Reference 22) and support recent studies in marmosets.[9] Often, animals had comparable peripheral viral kinetics but varying degrees of liver damage, irrespective of inoculation dose and time point post-infection. Tamarins S2 and S3 (twins) displayed comparable viremia profiles yet only S2 developed extensive liver damage and fibrosis. Thus, peripheral viral load is not a reliable indicator of the hepatic immune response.

To mimic the scenario in which individuals infected by HCV may undergo subsequent exposures to virus we challenged ten tamarins with a dose of virus equivalent to the original inoculum and assessed the effect on the liver. Compared to primary infection, secondary peripheral viremia is readily controlled, consistent with Bukh et al[3]; we also observed effective clearance of vRNA from the tissue. Yet, despite the absence of high vRNA levels, following rechallenge with 10^7 ge GBV-B three tamarins showed extensive immunopathological liver damage; the remaining three had mild damage and lymphocyte infiltrate. It is possible that the 10^7 ge dose was sufficiently high that damage occurring following primary infection was exacerbated upon challenge, but as one animal receiving 10^5 ge showed comparable morphological damage, that the damage is dose-related is not conclusive. This highlights that an appropriately designed vaccine should be able to minimize, if not prevent, the impact of the virus on the liver.

Of particular interest, we report fibrosis in male red-bellied tamarins. A link between fibrosis and gender in HCV-infected individuals suggested that males are more susceptible to liver damage than are premenopausal females[23]; this may be reflected in this red-bellied tamarin model where all four fibrotic animals were male. Virus-associated fibrosis was dependent on measurable viremia but was not restricted to those animals receiving the higher inoculum, nor did fibrosis development correlate absolutely with advanced liver damage. It has been postulated that elevated $CD8^+$ T cells in the liver of a HCV-infected individual contribute to cytopathic damage more than the virus itself thus leading to fibrosis.[24-27] By contrast, of the five tamarins in this study with elevated CD8-stained cells, two displayed naïve liver morphology. Furthermore, CD8 staining did not always correlate with raised cell proliferation marker levels. These observations suggest that the cause of bystander damage is not limited to $CD8^+$ T cells alone though we cannot exclude the possibility that CD8-stained cells were masked by extensive immune and EME infiltration. Furthermore, damage may also be caused by activated macrophages which, in response to IFN-γ release, develop into antigen-presenting cells (APC) leading to an increase in MHC class II presentation to $CD4^+$ T cells.[28,29] The development of fibrosis may be a cause of the ongoing immune response observed in the tamarins that had seemingly eliminated peripheral viremia; close proximity of NK cells and stellate cells allows for control of the latter in driving liver fibrosis (reviewed in Reference 30). Those animals displaying signs of fibrosis and exhibiting an immune response, despite peripheral clearance of viremia, also had sinusoidal immune infiltrate most likely comprising NK cells.[7] Since only some of these animals had detectable intrahepatic GBV-B vRNA, this ongoing immune response might not be directed against the vRNA but instead a response to limit the formation of fibrosis. While animals that displayed fibrosis had extensive immune infiltration, the reverse was not the rule: the presence of extensive infiltrate did not necessarily lead to fibrosis; for example, the female T18 had such infiltrate but no evidence of fibrotic tissue.

The availability of direct-acting antiviral drugs is a key step forward in the management of advanced HCV infections while a vaccine would have a major impact on the worldwide disease burden. Understanding the impact of infection on the liver would inform therapeutic development and applications thus knowledge of when and how liver morphology could be compromised is crucial for effective clinical intervention. By infecting red-bellied tamarins with an hepacivius closely related to HCV, we found that liver morphology is altered soon after infection and fibrosis can develop in this species. This model offers another attractive system for the testing of prophylactic and therapeutic treatments and the evaluation of their utility in preventing or reversing liver pathology that may develop in early infection. Our data add to the corpus of comparative GBV-B pathology in New World primates and particularly complement those reported for the *Callithrix jacchus*, common marmoset, model. Our data support the importance of the *Saguinus labiatus* and *Callithrix* models of HCV infection in man. Understanding the similarities and differences in hepacivirus-associated pathology in these species will optimize the selection of models for specific studies thereby in part addressing the 3Rs in animal research. GBV-B infection of the tamarin typically yields greater peak viral titers than does the marmoset, and its larger size, allowing for greater clinical sample size and collection frequency and obviating the need for serial sacrifice, may enhance its suitability as a model for acute infection assessment and vaccine evaluation. The smaller common marmoset has advantages as a tractable model for antiviral development and assessment.

In conclusion, we provide the first description of the development of liver pathology in red-bellied tamarins through successive time points in primary and secondary infections, which has implications on identifying clinically critical windows in which HCV-infected individuals could be treated to minimize liver damage. While longer-term studies are required to determine whether GBV-B replicates in the liver for protracted periods to establish a true occult infection, as has been reported for the common marmoset[9] we have demonstrated that an infection may persist in the liver in the absence of

detectable virus in the serum. To our knowledge this is the first report of fibrosis in tamarins; it supports data observed in the common marmoset.[8,9,13,14] Our observation that fibrosis affects male tamarins over female animals, is novel and mirrors the gender bias seen in HCV-infected humans. Furthermore, this is evidence that fibrotic tissue can appear in acute infection; reversal of such pathology would be a valuable outcome of DAA. This further establishes the red-bellied tamarin this animal as an important surrogate model for early HCV pathology. We are now able to assess the efficacy of candidate vaccines and immunotherapeutic interventions against damage in virus-associated hepatitis, both of which are an unmet need in the context of HCV infection in man.

ACKNOWLEDGMENTS

We would like to thank the veterinary and support staff for their expertise; D Ferguson for initial instruction in immunohistochemistry and E Mee for assistance with the figures. Financial support was awarded in part by EUPRIM-Net II, an EU FP7 grant and the UK Medical Research Council Grant number, G0900861. The funders had no role in study design, data collection and interpretation, decision to publish, or preparation of the manuscript.

ORCID

Nicola J. Rose http://orcid.org/0000-0003-1102-5062

REFERENCES

1. Bukh J, Apgar CL, Govindarajan S, Purcell RH. Host range studies of GB virus-B hepatitis agent, the closest relative of hepatitis C virus, in New World monkeys and chimpanzees. *J Med Virol*. 2001;65:694-697.
2. Manickam C, Reeves RK. Modeling HCV disease in animals: virology, immunology and pathogenesis of HCV and GBV-B infections. *Front Microbiol*. 2014;5:690.
3. Bukh J, Engle RE, Govindarajan S, Purcell RH. Immunity against the GBV-B hepatitis virus in tamarins can prevent productive infection following rechallenge and is long-lived. *J Med Virol*. 2008;80:87-94.
4. Bright H, Carroll AR, Watts PA, Fenton RJ. Development of a GB virus B marmoset model and its validation with a novel series of hepatitis C virus NS3 protease inhibitors. *J Virol*. 2004;78:2062-2071.
5. Jacob JR, Lin KC, Tennant BC, Mansfield KG. GB virus B infection of the common marmoset (*Callithrix jacchus*) and associated liver pathology. *J Gen Virol*. 2004;85:2525-2533.
6. Woollard DJ, Haqshenas G, Dong X, Pratt BF, Kent SJ, Gowans EJ. Virus-specific T-cell immunity correlates with control of GB virus B infection in marmosets. *J Virol*. 2008;82:3054-3060.
7. Hood SP, Mee ET, Perkins H, et al. Changes in immune cell populations in the periphery and liver of GBV-B-infected and convalescent tamarins (*Saguinus labiatus*). *Virus Res*. 2014;179:93-101.
8. Manickam C, Rajakumar P, Wachtman L, et al. Acute liver damage associated with innate immune activation in a small nonhuman primate model of hepacivirus infection. *J Virol*. 2016;90:9153-9162.
9. Manickam C, Martinot AJ, Jones RA, Varner V, Reeves RK. Hepatic immunopathology during occult hepacivirus re-infection. *Virology*. 2017;512:48-55.
10. Karayiannis P, Petrovic LM, Fry M, et al. Studies of Gb Hepatitis agent in tamarins. *Hepatology*. 1989;9:186-192.
11. Martin A, Bodola F, Sangar DV, et al. Chronic hepatitis associated with GB virus B persistence in a tamarin after intrahepatic inoculation of synthetic viral RNA. *Proc Natl Acad Sci USA*. 2003;100:9962-9967.
12. Ishii K, Iijima S, Kimura N, et al. GBV-B as a pleiotropic virus: distribution of GBV-B in extrahepatic tissues in vivo. *Microbes Infect*. 2007;9:515-521.
13. Iwasaki Y, Mori K, Ishii K, et al. Long-Term Persistent GBV-B infection and development of a chronic and progressive hepatitis C-like disease in marmosets. *Front Microbiol*. 2011;2:240.
14. Li T, Zhu S, Shuai L, et al. Infection of common marmosets with hepatitis C virus/GB virus-B chimeras. *Hepatology*. 2014;59:789-802.
15. Zhu S, Li T, Liu B, et al. Infection of common marmosets with GB virus B chimeric virus encoding the major nonstructural proteins NS2 to NS4A of hepatitis C virus. *J Virol*. 2016;90:8198-8211.
16. Beames B, Chavez D, Guerra B, Notvall L, Brasky KM, Lanford RE. Development of a primary tamarin hepatocyte culture system for GB virus-B: a surrogate model for hepatitis C virus. *J Virol*. 2000;74:11764-11772.
17. Schomaker S, Warner R, Bock J, et al. Assessment of emerging biomarkers of liver injury in human subjects. *Toxicol Sci*. 2013;132:276-283.
18. Mitchell JL, Murrell CK, Auda G, Almond N, Rose NJ. Early immunopathology events in simian retrovirus, type 2 infections prior to the onset of disease. *Virology*. 2011;413:161-168.
19. Ishak K, Baptista A, Bianchi L, et al. Histological grading and staging of chronic hepatitis. *J Hepatol*. 1995;22:696-699.
20. Shin EC, Seifert U, Kato T, et al. Virus-induced type I IFN stimulates generation of immunoproteasomes at the site of infection. *J Clin Invest*. 2006;116:3006-3014.
21. Larrubia JR, Calvino M, Benito S, et al. The role of CCR5/CXCR3 expressing CD8+ cells in liver damage and viral control during persistent hepatitis C virus infection. *J Hepatol*. 2007;47:632-641.
22. Carreno V, Bartolome J, Castillo I, Quiroga JA. New perspectives in occult hepatitis C virus infection. *World J Gastroenterol*. 2012;18:2887-2894.
23. Villa E, Karampatou A, Cammà C, et al. Early menopause is associated with lack of response to antiviral therapy in women with chronic hepatitis C. *Gastroenterology*. 2011;140:818-829.
24. Crispe IN. Do natural T cells promote liver regeneration? *Hepatology*. 2000;31:1022-1024.
25. Thimme R, Bukh J, Spangenberg HC, et al. Viral and immunological determinants of hepatitis C virus clearance, persistence, and disease. *Proc Natl Acad Sci USA*. 2002;99:15661-15668.
26. Bonacini M, Govindarajan S, Kohla M, Lai MM, Lindsay KL. Intrahepatic lymphocyte phenotypes in hepatitis C virus infection: a comparison between cirrhotic and non-cirrhotic livers. *Minerva Gastroenterol Dietol*. 2007;53:1-7.
27. Feuth T, Arends JE, Fransen JH, et al. Complementary role of HCV and HIV in T-cell activation and exhaustion in HIV/HCV coinfection. *PLOS One*. 2013;8:e59302.
28. Burgio VL, Ballardini G, Artini M, Caratozzolo M, Bianchi FB, Levrero M. Expression of co-stimulatory molecules by Kupffer cells in chronic hepatitis of hepatitis C virus etiology. *Hepatology*. 1998;27:1600-1606.
29. Heydtmann M. Macrophages in hepatitis B and hepatitis C virus infections. *J Virol*. 2009;83:2796-2802.
30. Rehermann B. Pathogenesis of chronic viral hepatitis: differential roles of T cells and NK cells. *Nat Med*. 2013;19:859-868.

SUPPORTING INFORMATION

Additional supporting information may be found online in the Supporting Information section.

How to cite this article: Dale JM, Hood SP, Bowen O, et al. Development of hepatic pathology in GBV-B-infected red-bellied tamarins (*Saguinus labiatus*). *J Med Virol*. 2020;1–12. https://doi.org/10.1002/jmv.25769